processes

MDPI

Article

A New Predictive Model for Open-Hole Wellbore Stability During the Production Phase of Ultra-Deep Extended-Reach Wells Based on Critical Production Pressure Difference Constraints

Junrui Ge [1,2], Gengchen Li [2,*], Yanfei Li [1], Bin Cai [1], Xuyue Chen [2,*], Jin Yang [2], Tianwei Chen [2] and Jun Zeng [2]

[1] CNOOC Limited, Shanghai 200335, China; gejr@cnooc.com.cn (J.G.); liyf8@cnooc.com.cn (Y.L.); caibin4@cnooc.com.cn (B.C.)
[2] MOE Key Laboratory of Petroleum Engineering, China University of Petroleum, Beijing 102249, China; yjin@cup.edu.cn (J.Y.); davidchen2001@163.com (T.C.); zengjunzero@163.com (J.Z.)
* Correspondence: 2022215866@student.cup.edu.cn (G.L.); chenxuyue2011@163.com (X.C.)

Abstract

This study investigates wellbore stability in ultra-deep extended-reach wells (ERWs) in the East China Sea, where perforated pipes (a type of screen completion) are commonly used to support wellbore walls and prevent collapse. Cost constraints sometimes lead to the omission of this support, yet significant wellbore collapse is rarely observed. The instability is primarily attributed to variations in production pressure differences. A predictive model for critical pressure difference was developed based on immersion experiments and single-triaxial rock mechanics tests. The results from immersion tests revealed that, in water-bearing strata, the critical pressure difference decreased significantly, drop-ping by 20.07% after two days of rock core immersion and by 28.35% after seven days. Key factors influencing this difference, such as well inclination, rock cohesion, internal friction angle, Poisson's ratio, and Biot coefficient, were identified. As production continues, pore pressure depletion reduces this difference, particularly when pore pressure falls below 23.5 MPa, leading to wellbore instability. On-site validation in three ultra-deep ERWs showed that the model's predictions aligned well with actual conditions, with a confidence interval analysis further validating the model's accuracy. The proposed model provides valuable guidance for future ultra-deep well development in the East China Sea.

Keywords: ultra-deep extended-reach wells; oil and gas production; open-hole wellbore stability; critical production pressure difference

Academic Editor: Michael C. Georgiadis

Received: 24 September 2025
Revised: 13 October 2025
Accepted: 17 October 2025
Published: 21 October 2025

Citation: Ge, J.; Li, G.; Li, Y.; Cai, B.; Chen, X.; Yang, J.; Chen, T.; Zeng, J. A New Predictive Model for Open-Hole Wellbore Stability During the Production Phase of Ultra-Deep Extended-Reach Wells Based on Critical Production Pressure Difference Constraints. *Processes* **2025**, *13*, 3373. https://doi.org/10.3390/pr13103373

1. Introduction

The exploration and development of offshore oil and gas resources are increasingly being directed toward deep and ultra-deep areas. The oil and gas resources in the East China Sea have been identified as one of the key strategic areas for offshore exploration and development in China. Since exploration was initiated in the mid-1970s, substantial progress has been achieved in the evaluation of low-permeability tight sandstone gas reservoirs within the East China Sea. The East China Sea has huge gas reservoir resource potential and is one of the most important oil- and gas-rich areas in China [1,2]. The reservoir is characterized by typical low-porosity, low-permeability, and high-water-saturation properties, which present numerous challenges during production operations [3–5]. The complex geological

conditions of the East China Sea Basin, particularly the high temperature, high horizontal stress, and tight rock characteristics, pose significant challenges to wellbore stability during the production phase of ultra-deep ERWs [6]. During production, the long-term weakening effect of formation water on rock strength, along with pore pressure depletion, increases the risk of wellbore collapse and shear failure. The sandstone formations in the study area, though mechanically strong, have low porosity and permeability, which limits fluid flow and further exacerbates the risks to wellbore stability during production.

In this context, ERWs and cluster wells have been increasingly adopted as preferred development solutions in this region, primarily due to their ability to resolve offshore land-use conflicts, enable distal reservoir access from single platforms, and generate substantial economic returns. From an engineering perspective, open-hole completion technology has been widely implemented in East China Sea ultra-deep ERWs to enhance hydrocarbon productivity while reducing operational expenditures, owing to the complex subsurface environment [7,8]. Nevertheless, wellbore collapse incidents have been observed in certain well sections during production phases, typically necessitating the installation of perforated pipes for wellbore support. In this study, a perforated pipe refers to a pipe with perforations that creates a fluid passage between the wellbore and the formation; they are mainly used in open-hole completions and provide support to prevent wellbore collapse during production. In contrast, screen completion involves installing a sand control screen to prevent sand particles from entering the wellbore, protecting equipment and pipes. We provide a clear definition of "perforated pipe" when it first appears to distinguish the two concepts. Notably, many ultra-deep ERWs have been successfully completed without perforated pipe deployment. Field production data have demonstrated that these wells maintain stable wellbore conditions while achieving considerable hydrocarbon output and economic benefits. Conventional wellbore stability analysis methods are generally based on the premise of the drilling fluid pressure balancing the pore pressure. However, this approach becomes problematic when applied to gas wells, which are predominant in the East China Sea, where wellbores are gas-filled during production. Consequently, reliable evaluation criteria for open-hole stability during production in ultra-deep ERWs remain to be established, highlighting a critical research gap that needs to be addressed for future engineering design optimization and operational planning.

Significant research efforts have been devoted to investigating open-hole wellbore stability by scholars worldwide. A semi-analytical solution model was developed by Aadnoy [9], incorporating the anisotropic elastic properties, directional shear, and directional tensile strength of the wellbore-surrounding formation. This model was subsequently enhanced by See Hong Ong [10], who established a stress calculation model for anisotropic formations. The stability of the wellbore was evaluated using a three-dimensional anisotropic strength failure criterion, with particular attention given to wellbore collapse phenomena in anisotropic formations. Lee [11] combined the strength of isotropic and anisotropic rocks and the stress state around the wellbore, considered two kinds of shear failure modes, and established a wellbore stability model to evaluate the influence of in situ stress, weak plane and wellbore trajectory on the wellbore stability of drilling into thin layers. He [12] introduced a new wellbore stability model considering a weak bedding plane, analyzed the geometric relationship between the weak bedding plane and wellbore, and the influence of weak bedding plane parameters and in situ stress on wellbore stability. Li [13] established a new wellbore stability analysis model for transversely isotropic shale formations by considering the influence of transversely isotropic characteristics of shale on stress concentration and combining the changes of tensile breakdown and shear collapse criteria. Li [14] proposed a three-dimensional wellbore stability model considering thermal stress by analyzing the temperature sensitivity of horizontal drilling combined with the circulation

temperature model. He [15] analyzed the influence of water-based drilling fluid on shale strength and failure mode through mechanical experiments and established a wellbore stability model for shale formations. Zhou [16] studied the influence of anisotropic seepage and weak bedding plane on wellbore stability during horizontal well drilling. Wei [17] overcame the wall instability of the F7H well in the Dongfang gas field, South China Sea, by improving the structure of the suspended packer and closely monitoring the wellbore condition, in addition to completing the high-temperature and high-pressure small-borehole perforated pipe lowering operation. Fu [18] used numerical modeling combined with the Drucker–Prager strength criterion and effective plastic strain criterion to simulate and analyze the influence of production pressure difference on the stability of fractured wellbore, in addition to establishing a design method for the completion fluid density for ultra-deep wells in horizontal section of long open hole based on wellbore stability control. Based on the 'C' formula method, Huang [19] introduced the additional stress of oil and gas seepage, established the calculation model of wellbore circumferential stress, and proposed an improved wellbore stability evaluation method. Sun [20] determined the salinity of drilling mud to control the amount of free gas produced by marine GHBS, thereby strengthening the stability of the wellbore. Wang [21] found that the use of colder wellbore fluid can move the maximum tangential stress on the wellbore wall into the stratum. Ma [22] found through experiments that the traditional Mohr–Coulomb criterion is too conservative in predicting wellbore stability, and the minimum safe molecular weight predicted by the innovative integrated breakthrough width model and the Mogi–Coulomb criterion is the closest to reality. Guo [23] proposed a new elastic–plastic analysis solution for the wellbore stability of MHBS drilling by combining the reduction in stratum stiffness and strength after hydrate dissociation and the partial coupling between seepage, temperature, salt concentration and the mechanical field. Liu [24] tested the physical, chemical and mechanical properties of Longmaxi Formation shale soaked in different working fluids through experiments, establishing a theoretical model to evaluate the wellbore stability of shale under different working conditions of drilling, fracturing and completion. Liu [25] constructed a three-dimensional creep equation by extending the one-dimensional creep equation and combining the viscoelastic–plastic characteristics and damage effects. Yousefian [26] used boundary element numerical code to simulate the formation process of drilling holes after 20 steps of fracture propagation in a shaft in southwestern Iran; they found that a very narrow and unclear breakthrough area can be predicted using numerical simulation and FMI data. Rashidi [27] focused on the risk of instability in the long-term injection of CO_2 in the open hole section and used the thermal–fluid–solid unidirectional coupling dynamic geomechanical model to evaluate the integrity of the open-hole completion section in the full cycle of CO_2 injection. Chen [28] established a model for MSE prediction during horizontal section drilling of horizontal wells. Merey [29] described the special completion operations of cementing, perforating, sand screening, and completion strings during the completion of natural gas hydrate wells, which provide a reference for equipment design during drilling and completion of wells in natural gas hydrate reservoirs. However, the existing research, as reviewed above, primarily focuses on wellbore stability during the drilling phase, with comprehensive models and criteria established for scenarios where wellbores are filled with drilling fluid. A significant research gap remains regarding the stability of open-hole wellbores during the production phase of ultra-deep ERWs, especially in gas reservoirs where the wellbore is gas-filled and the support from drilling fluid is absent. Furthermore, the long-term weakening effect of formation water on rock strength and the evolution of in situ stress due to pore pressure depletion over the production life cycle are often not adequately integrated into existing models.

To address these gaps, this study aims to: (1) Quantify the time-dependent weakening of rock mechanical parameters due to formation water immersion through laboratory experiments; (2) Develop a novel predictive model for the critical production pressure difference that incorporates the effects of thermal stress, pore pressure depletion, and the evolution of in-situ stress around the wellbore. The critical production pressure difference refers to the maximum pressure difference that the wellbore can withstand during production. If this value is exceeded, the wellbore may collapse or fail. The model predicts this maximum value to ensure that the actual pressure difference during production does not exceed it, thereby maintaining wellbore stability; (3) Identify and analyze the sensitivity of key parameters influencing wellbore stability during production; (4) Validate the model's accuracy and engineering applicability using field data from three ultra-deep ERWs in the East China Sea. The findings of this research are expected to provide a theoretical basis and technical support for optimizing the production and development of ultra-deep ERWs.

2. Rock Mechanics and Immersion Experiments

In the completion and production stages, the main rock mechanics parameters involved in the study of wellbore stability in the production stage of ultra-deep ERWs include compressive strength, elastic modulus, Poisson's ratio, cohesion, internal friction angle, etc. These parameters jointly characterize the strength characteristics, deformation behavior and failure mechanism of rocks under external forces. In order to study the wellbore stability of low-permeability oil and gas reservoirs in the East China Sea during the production stage, considering the interaction between strata water and surrounding rock during the production process, this study selected the H3b core to carry out rock mechanics experiments. The cores collected on site were soaked in simulated strata water, and the relevant mechanical performance parameters were analyzed. The experimental core photos are shown in Figure 1, and the strata water preparation experiment is shown in Figure 2. The experimental data obtained are shown in Table 1.

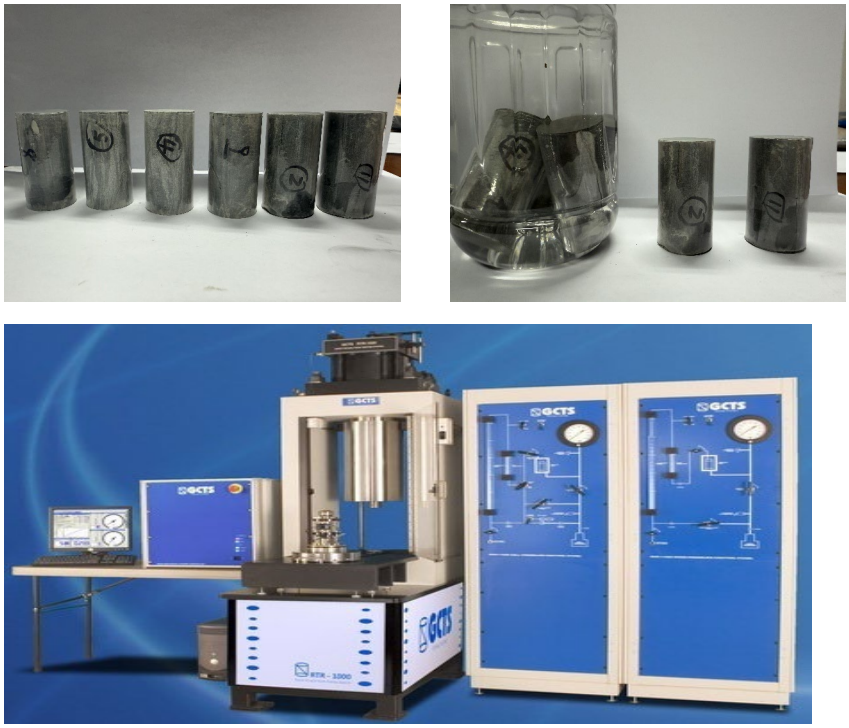

Figure 1. Preparation of rock mechanics experiment and RTR-1000 true triaxial rock mechanics test machine.

(**a**) (**b**)

Figure 2. Preparation diagram of strata water experiment. (**a**) Chemical reagents for the actual formation water compatibility experiment. (**b**) Completed configuration diagram of the formation water experiment.

Table 1. Parameter diagram of rock mechanics experiment.

Core No.	Length (mm)	Diameter (mm)	Quality (g)	Density (g/cm^3)	Confining Pressure (Mpa)	Compressive Strength (Mpa)	Elastic Modulus (Gpa)	Poisson Ratio	Cohesion (Mpa)	Angle of Internal Friction (°)	Remark
1	46.74	25.43	57.14	2.41	0	101.9	21.3	0.329	21.02	45.15	unsoaked
2	42.94	25.43	52.35	2.40	30	278.1	39.0	0.237			
3	46.76	25.42	56.87	2.40	0	86.5	20.2	0.348	17.50	45.94	soak for 48 h
4	46.77	25.44	57.37	2.41	30	269.7	34.8	0.292			
5	46.78	25.41	57.67	2.43	0	80.5	19.2	0.387	16.41	45.64	soak for 168 h
6	46.68	25.45	57.32	2.42	30	261.0	34.2	0.349			

The relevant rock cores are divided into three groups: the dry group remained in the original unsoaked state; immersion group I was immersed in simulated strata water with a salinity of 10,000 mg/L for 48 h; immersion group II was immersed in the same simulated strata water for 168 h (seven days). After soaking, uniaxial compression tests and triaxial compression tests were conducted on the three core samples. The experimental results were used to fit the final rock strength after stabilization under the influence of water soaking. The results are shown in Figure 3.

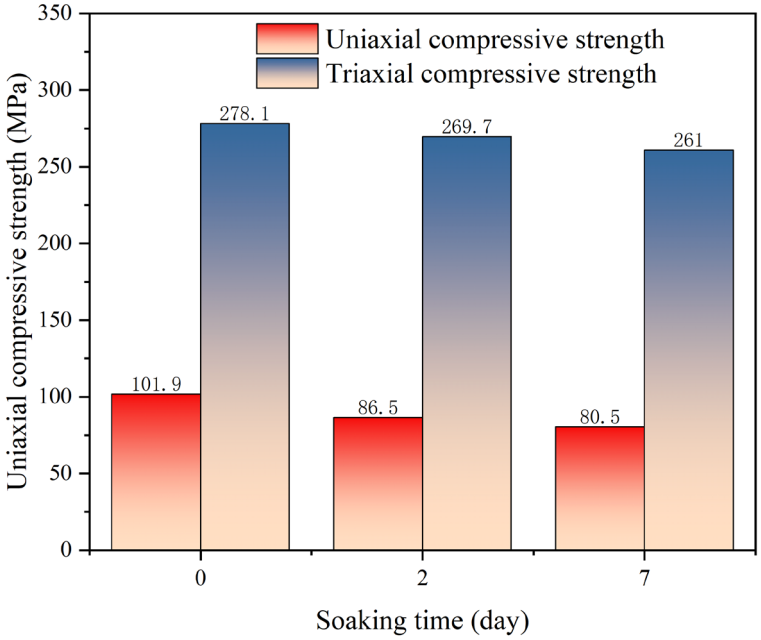

Figure 3. Changes of uniaxial and triaxial compressive strength with soaking time.

By comparing and analyzing the strength parameters of rock after different soaking times, it is determined that the soaking of strata water has a significant weakening effect on rock strength, and this weakening effect began to appear in the early stage of 48 h soaking; it tends to be relatively stable after 168 h of complete exposure to water. The uniaxial compressive strength of the strata rock decreased from 101.09 MPa to 80.5 MPa, and the triaxial compressive strength decreased from 269.7 MPa to 259 MPa. Strata water immersion cannot indefinitely weaken the compressive strength of rocks. The uniaxial compressive strength decreased to 79.63%, and the triaxial compressive strength decreased to 96.28%. The effect of exposing the core completely to water on uniaxial compressive strength is even more pronounced. This is mainly because, under triaxial stress conditions, the presence of confining pressure partially inhibits the physical and chemical softening effect of water on the internal structure of rocks, whereas, under uniaxial stress conditions without confining pressure, the weakening effect of water is more fully manifested.

3. Critical Production Pressure Difference Model

First, through field research, it was found that the geothermal gradient in the East China Sea geological conditions exceeds 3.7 °C/100 m, and the target stratum depth exceeds 3800 m, which constitutes a high-temperature stratum. Due to the temperature difference generated in the wellbore, according to the theory of thermal elasticity, the additional thermal stress on the wellbore wall caused by temperature changes can be expressed by Equation (1) [30]:

$$\begin{aligned} \sigma_{rr}^{T} &= K \cdot \frac{1}{r^2} \int_{r_w}^{r} \Delta T(r') \cdot r' dr' \\ \sigma_{\theta\theta}^{T} &= -K \left[\frac{1}{r^2} \int_{r_w}^{r} \Delta T(r') \cdot r' dr' - \Delta T(r) \right] \\ \sigma_{zz}^{T} &= K \cdot \Delta T \end{aligned} \tag{1}$$

where σ_{rr}^{T} is the radial stress caused by temperature change in the wellbore; $\sigma_{\theta\theta}^{T}$ is the hoop stress caused by temperature change in the wellbore; σ_{zz}^{T} is the axial stress caused by temperature change in the wellbore; r' is the radial distance, m; ΔT is temperature change during the production process, MPa/°C; and K is the temperature effect coefficient, MPa/°C.

K can be expressed by Equation (2):

$$K = \frac{E_t \alpha_T}{3(1 - \nu_t)} \tag{2}$$

The parameters E_t and ν_t, which change with the soaking time of the formation water, were obtained through a binomial fit shown in Table 1.

$$E_t = 39 - 2.66517\mathrm{t} - 0.28286\mathrm{t}^2 \tag{3}$$

$$\nu_t = 0.237 + 0.0321\mathrm{t} - 0.0023\mathrm{t}^2 \tag{4}$$

where E_t is the Young's modulus with the soaking time of formation water, α_T is the volumetric thermal expansion coefficient of the rock matrix, and ν_t is s Poisson's ratio with the soaking time of formation water.

It should be noted that, under typical conditions, the reservoir does not come into contact with formation water. Therefore, in standard production scenarios, the rock strength is generally not weakened by soaking. For this reason, the effects of soaking on rock strength degradation are not considered in the subsequent calculations. This simplification is deemed reasonable for the scope of this study and does not significantly impact the primary estimation of the critical drawdown pressure.

However, due to depletion of the reservoir during the later stages of production, changes in pore pressure have a significant impact on in situ stress, which can be expressed by the following equation:

$$\Delta\sigma_H = \Delta\sigma_h = \alpha_p \frac{1-2v}{1-v}\Delta p_p \tag{5}$$

where Δp_p is the change value of the pore pressure caused by the exhaustion of pore pressure, $\Delta\sigma_H$ is the change value of maximum horizontal in situ stress caused by the exhaustion of pore pressure, and $\Delta\sigma_h$ is the change value of minimum horizontal in situ stress caused by the exhaustion of pore pressure.

As shown in the Figure 4, the formulas for calculating the overburden pressure, maximum horizontal in situ stress, and minimum horizontal in situ stress in the global coordinate system are given by Equations (6)–(8). According to the geological characteristics of East China Sea and the experience of similar reservoirs, the effective stress coefficient of the target sandstone reservoir is generally in the range of 0.90~0.95:

$$\sigma_v = \int_0^H \rho(h) g dh \tag{6}$$

$$\sigma_H = \left(\frac{u_s}{1-u_s} + \mathrm{str}_1\right)(\sigma_v - \alpha_p P_p) + \alpha_p P_p + \Delta\sigma_H \tag{7}$$

$$\sigma_h = \left(\frac{u_s}{1-u_s} - \mathrm{str}_2\right)(\sigma_v - \alpha_p P_p) + \alpha_p P_p + \Delta\sigma_h \tag{8}$$

where σ_v is overburden pressure, σ_H is the maximum horizontal in situ stress caused by the exhaustion of pore pressure, σ_h is the minimum horizontal in situ stress caused by the exhaustion of pore pressure, and α_p is Biot's parameter.

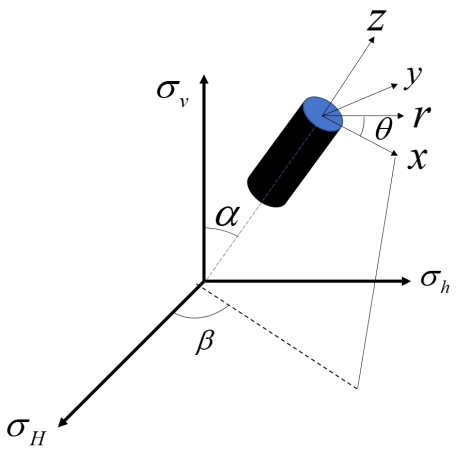

Figure 4. The conversion of coordinates and stress distribution around the wellbore: coordinate conversion for deviated wellbore [31].

As shown in the Figure 5, the vertical stress and the maximum and minimum horizontal in situ stress in the principal stress coordinate system (x', y', z') are transformed into the component of the stress around the well in the axial coordinate system (x, y, z) [31–33]:

$$\begin{pmatrix} \sigma_{xx} & \tau_{xy} & \tau_{xz} \\ \tau_{yx} & \sigma_{yy} & \tau_{yz} \\ \tau_{zx} & \tau_{zy} & \sigma_{zz} \end{pmatrix} = [L] \begin{pmatrix} \sigma_H & & \\ & \sigma_h & \\ & & \sigma_z \end{pmatrix} [L]^T \tag{9}$$

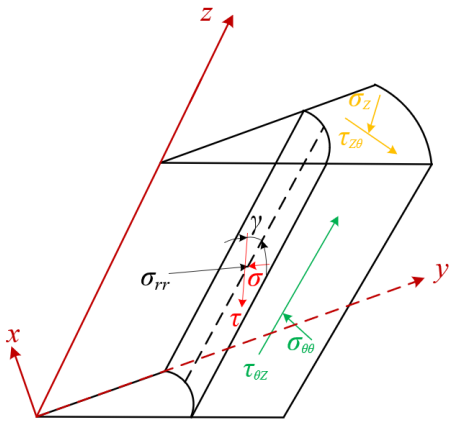

Figure 5. The conversion of coordinates and stress distribution around the wellbore: principle stresses at the wellbore wall [31].

The expression for L is as follows:

$$L = \begin{pmatrix} \cos\alpha\cos\beta & \cos\alpha\sin\beta & -\sin\beta \\ -\sin\beta & \cos\beta & 0 \\ \sin\alpha\cos\beta & \sin\alpha\cos\beta & \cos\beta \end{pmatrix} \tag{10}$$

Through mathematical deduction:

$$\begin{cases} \sigma_{xx} = \sigma_H\cos^2\alpha\cos^2\beta + \sigma_h\cos^2\alpha\sin^2\beta + \sigma_v\sin^2\alpha \\ \sigma_{yy} = \sigma_H\sin^2\beta + \sigma_h\cos^2\beta \\ \sigma_{zz} = \sigma_H\sin^2\alpha\cos^2\beta + \sigma_h\sin^2\alpha\sin^2\beta + \sigma_v\cos^2\alpha \\ \tau_{xy} = -\sigma_H\cos\alpha\cos\beta\sin\beta + \sigma_h\cos\alpha\cos\beta\sin\beta \\ \tau_{xz} = \sigma_H\cos\alpha\cos\alpha\cos^2\beta + \sigma_h\cos\alpha\sin\alpha\sin^2\beta \\ \tau_{yz} = -\sigma_H\sin\alpha\cos\beta\sin\beta + \sigma_h\sin\psi\cos\beta\sin\beta \end{cases} \tag{11}$$

where σ_{xx}, σ_{yy}, σ_{zz} are x', y', and z' axial stresses in local wellbore coordinate, respectively, and τ_{xy}, τ_{xz}, τ_{yz} are three components of shear stresses in local wellbore coordinate.

After the linear superposition treatment, the stress around the ERW considering the influence of temperature effect and pore pressure failure can be expressed as follows:

$$\begin{cases} \sigma_{rr} = \dfrac{R^2}{r^2}p_w + \dfrac{(\sigma_{xx}+\sigma_{yy})}{2}(1-\dfrac{R^2}{r^2}) + \dfrac{(\sigma_{xx}-\sigma_{yy})}{2}(1+\dfrac{3R^4}{r^4}-\dfrac{4R^2}{r^2})\cos 2\theta \\ +\sigma_{xy}(1+\dfrac{3R^4}{r^4}-\dfrac{4R^2}{r^2})\sin 2\theta + K\cdot\dfrac{1}{r^2}\int_{r_w}^{r}\Delta T(r')\cdot r'dr' \\ \sigma_{\theta\theta} = \dfrac{R^2}{r^2}p_w + \dfrac{(\sigma_{xx}+\sigma_{yy})}{2}(1+\dfrac{R^2}{r^2}) - \dfrac{(\sigma_{xx}-\sigma_{yy})}{2}(1+\dfrac{3R^4}{r^4})\cos 2\theta - \\ \sigma_{xy}(1+\dfrac{3R^4}{r^4})\sin 2\theta - K\left[\dfrac{1}{r^2}\int_{r_w}^{r}\Delta T(r')\cdot r'dr' - \Delta T(r)\right] \\ \sigma_{zz} = \sigma_{zz} - \nu\left[2(\sigma_{xx}-\sigma_{yy})(\dfrac{R}{r})^2\cos 2\theta + 4\sigma_{xy}(\dfrac{R}{r})^2\sin 2\theta\right] + K\cdot\Delta T \\ \tau_{r\theta} = \dfrac{(\sigma_{yy}-\sigma_{xx})}{2}(1-\dfrac{3R^4}{r^4}+\dfrac{2R^2}{r^2})\sin 2\theta + \sigma_{xy}(1-\dfrac{3R^4}{r^4}+\dfrac{2R^2}{r^2})\cos 2\theta \\ \tau_{\theta z} = \sigma_{yz}(1+\dfrac{R^2}{r^2})\cos\theta - \sigma_{xz}(1+\dfrac{R^2}{r^2})\sin\theta \\ \tau_{zr} = \sigma_{xz}(1-\dfrac{R^2}{r^2})\cos\theta + \sigma_{yz}(1-\dfrac{R^2}{r^2})\sin\theta \end{cases} \tag{12}$$

where σ_{rr} is the radial stress around the wellbore including the temperature and exhaustion of pore pressure's effects, $\sigma_{\theta\theta}$ is the hoop stress around the wellbore including the temperature and exhaustion of pore pressure's effects, σ_{zz} is axial stress around the wellbore including the temperature and exhaustion of pore pressure's effects, $\tau_{r\theta}$, $\tau_{\theta z}$, τ_{zr} are three

components of shear stress around the wellbore including the temperature and exhaustion of pore pressure's effects, and θ is the circumferential angle around the wellbore measured counter-clockwise from the x-axis.

In the wellbore, the stress component of the wellbore considering thermal stress and pore pressure depletion is expressed by Equation (13):

$$\begin{aligned} &\sigma_r = p_w - \delta\rho(p_w - p_p) \\ &\sigma_\theta = A\sigma_H + B\sigma_H + C\sigma_v + (K-1)p_w - Kp_p + S\Delta T \\ &\sigma_z = D\sigma_H + E\sigma_H + F\sigma_v + K(p_w - p_p) + S\Delta T \\ &\tau_{\theta z} = G\sigma_H + H\sigma_H + J\sigma_v \\ &\tau_{r\theta} = \tau_{rz} = 0 \end{aligned} \tag{13}$$

The coefficients A–J can be expressed by Equation (14):

$$\begin{cases} A = \cos^2\alpha\cos^2\gamma(1 - 2\cos 2\theta) + \sin^2\alpha(1 + 2\cos 2\theta) \\ +2\sin 2\alpha\sin 2\theta\cos\gamma \\ B = \sin^2\alpha\cos^2\gamma(1 - 2\cos 2\theta) + \cos^2\alpha(1 + 2\cos 2\theta) \\ -2\sin 2\alpha\sin 2\theta\cos\gamma \\ C = \sin^2\gamma(1 - 2\cos 2\theta) \\ D = \cos^2\alpha\sin^2\gamma(1 - 2\cos 2\theta) + 2\nu\cos 2\theta(\sin^2\alpha - \cos^2\alpha\cos^2\gamma) \\ +2\nu\sin 2\theta\sin 2\alpha\cos\gamma \\ E = \sin^2\alpha\sin^2\gamma(1 - 2\cos 2\theta) + 2\nu\cos 2\theta(\cos^2\alpha - \sin^2\alpha\cos^2\gamma) \\ -2\nu\sin 2\theta\sin 2\alpha\cos\gamma \\ F = \cos^2\gamma - 2\nu\cos 2\theta\sin^2\gamma \\ G = -\cos^2\alpha\sin 2\gamma\sin\theta - \cos\gamma\sin 2\alpha\sin 2\theta \\ H = -\sin^2\alpha\sin 2\gamma\sin\theta + \cos\gamma\sin 2\alpha\sin 2\theta \\ J = \sin 2\gamma\sin\theta \\ S = \delta\left[\frac{\alpha_p(1-2\nu)}{1-\nu} - \varphi\right] \end{cases} \tag{14}$$

where A–J are the factors of coordinate conversion.

As shown in the diagram, the radial stress σ_{rr} is the main stress, and the normal stress σ and tangential stress τ at an angle γ to the z-axis can be expressed by Equation (15):

$$\begin{cases} \sigma = \sigma_{\theta\theta}\cos^2\gamma + 2\tau_{rz}\cos\gamma\sin\gamma + \sigma_{zz}\sin^2\gamma \\ \tau = 0.5(\sigma_{zz} - \sigma_{\theta\theta})\sin 2\gamma + \tau_{rz}\cos 2\gamma \end{cases} \tag{15}$$

where γ is the angle between the Z axis and the normal stress, σ is the normal stress, and $\tau$is the shear stress.

In order to calculate the principal stress, let $\frac{d\sigma}{d\gamma} = 0$. Thus, we obtain Equation (16):

$$\begin{cases} \gamma_1 = \frac{1}{2}\arctan\frac{2\tau_{\theta z}}{\sigma_{\theta\theta} - \sigma_{zz}} \\ \gamma_2 = \frac{\pi}{2} + \frac{1}{2}\arctan\frac{2\tau_{\theta z}}{\sigma_{\theta\theta} - \sigma_{zz}} \end{cases} \tag{16}$$

Taking Equation (16) into Equation (15), three principal stresses on the inclined shaft wall of ultra-deep ERWs can be obtained:

$$\begin{cases} \sigma_i = \sigma_r = p_w \\ \sigma_j = \frac{1}{2}\left[X - \frac{2(1-2\nu)}{(1-\nu)}\alpha p_p + (\frac{2(1-2\nu)}{(1-\nu)}\alpha - 1)p_w + 2K\Delta T\right] \\ +\frac{1}{2}\sqrt{(Y - p_i)^2 + Z} \\ \sigma_k = \frac{1}{2}\left[X - \frac{2(1-2\nu)}{(1-\nu)}\alpha p_p + (\frac{2(1-2\nu)}{(1-\nu)}\alpha - 1)p_w + 2K\Delta T\right] \\ -\frac{1}{2}\sqrt{(Y - p_i)^2 + Z} \end{cases} \tag{17}$$

The three principal stress factors can be expressed by Equation (18):

$$\begin{aligned} X &= (A+D)\sigma_h + (B+E)\sigma_H + (C+F)\sigma_v \\ Y &= (A-D)\sigma_h + (B-E)\sigma_H + (C-F)\sigma_v \\ Z &= 4(GG\sigma_h + H\sigma_H + J\sigma_v)^2 \end{aligned} \tag{18}$$

where X, Y, and Z are three factors of principal stresses.

According to Mohr–Coulomb failure criterion, the minimum bottom hole flowing pressure to keep the wellbore from shear failure can be expressed by Equation (19):

$$\sigma_1 - \alpha p_p = (\sigma_3 - \alpha p_p)\frac{1+\sin\varphi}{1-\sin\varphi} + \frac{2c\cos\varphi}{1-\sin\varphi} \tag{19}$$

where σ_1 is the maximum value among σ_i, σ_j and σ_k, σ_3 is the minimum value among σ_i, σ_j and σ_k.

The critical production pressure difference that maintains the bare borehole wall stable open hole during the production stage can be expressed by Equation (20):

$$p_{\max-pro} = p_p - p_w \tag{20}$$

4. Model Validation and Example Analysis

As production time progresses, pore pressure depletion occurs, and the predicted pore pressure data from the field are incorporated into the model. The following data only consider changes in pore pressure. To validate the accuracy, reliability, and engineering applicability of the model for evaluating the stability of long horizontal wellbore walls established in this study, we selected three production wells ($X1$, $X2$, and $X3$) of the East China Sea that had been drilled, completed, and put into production as typical application cases for comparative analysis. All three wells encountered the target low-permeability sandstone reservoir and were completed using open-hole completion methods, but there were differences in completion protection measures and production pressure difference control, providing good comparison conditions for model verification. Using the model established in the previous section, the critical production pressure differences for wells $X1$, $X2$, and $X3$ were calculated. The established mathematical model was compared and verified with the actual measurement data from the field, and the results are shown in Figures 6–8. The 95% confidence band and 95% forecast band were generated using Origin software. The confidence band represents the possible range of the true regression line with 95% confidence, considering model errors; meanwhile, the forecast band represents the possible range for future observations, considering both model uncertainty and the inherent variability in the data. These bands were generated using the regression model applied in Origin software without employing Analysis of Variance (ANOVA), Monte Carlo simulations, or Bootstrap resampling methods.

Figure 6 shows that the actual production pressure difference of the $X1$ well is much lower than the calculated critical production pressure difference during the production date, and the perforation pipe is not put down for additional support when the well is completed. Throughout the production cycle, no obvious wellbore collapse or instability was observed by means of well logging, sand production monitoring and downhole television. The model predicts that the well has a high stability margin under a low production pressure difference, which is highly consistent with the actual production performance.

As shown in Figure 7, during the production period, the actual production pressure difference at well $X2$ exceeded the critical production pressure difference on multiple occasions. During the production testing phase of this well, noticeable signs of wellbore instability were detected, indicating a high risk of collapse. Based on model predictions and early production indicators, a perforated pipe was installed during actual construction to

provide radial support and enhance wellbore stability. After inserting the perforated pipe, signs of wellbore instability were effectively controlled. The model successfully predicted the risk of wellbore instability under high production pressure difference, consistent with the actual observed risks and the protective measures taken.

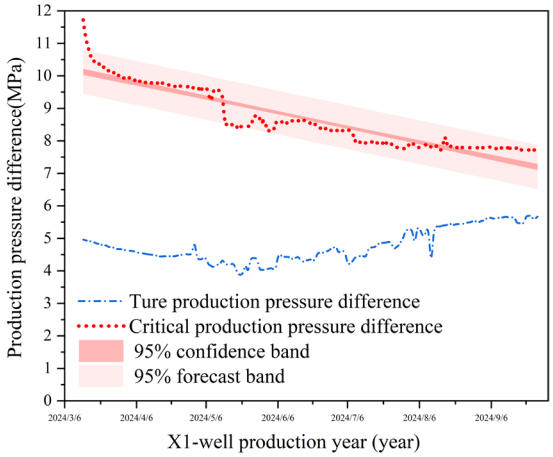

Figure 6. Comparison of actual production pressure difference and simulated critical production pressure difference in well *X*1.

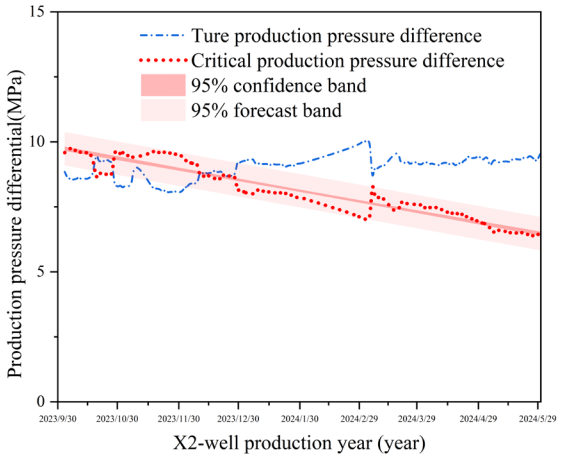

Figure 7. Comparison of actual production pressure difference and simulated critical production pressure difference in well *X*2.

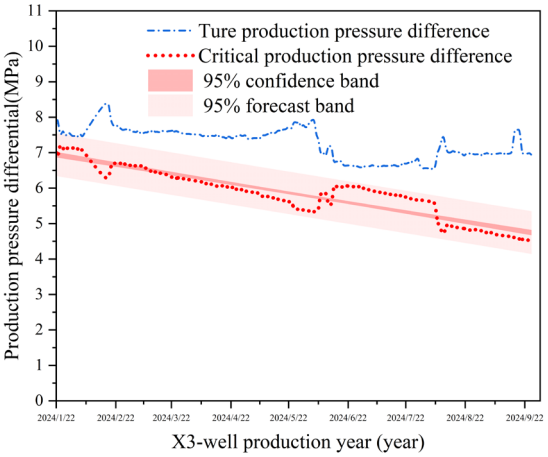

Figure 8. Comparison of actual production pressure difference and simulated critical production pressure difference in the *X*3 well.

As shown in Figure 8, during the production period, the actual pressure difference of *X*3 was close to the critical pressure difference. The model predicted that the well was in a critical stable state and had a certain risk of collapse. Based on the model assessment results, preventive measures were taken during the completion process by installing perforated pipes to prevent potential wellbore instability. The model accurately predicted that the well was in a stable boundary state, and the protective measures actually taken verified the risk assessment value of the model. After the perforated pipe was lowered, production was stable and no serious instability occurred. Comprehensive comparison results show that the model's prediction results are basically consistent with the actual situation on site, and it has good engineering applicability and guidance value.

5. Sensitivity Analysis of Critical Production Pressure Difference

The sensitivity of the critical production pressure difference for well *X*1 in the case study is explored based on the data in Table 2, where the true vertical depth, overburden pressure, maximum horizontal stress, minimum horizontal stress, pore pressure, angle between the azimuth of wellbore and the azimuth of maximum horizontal stress, and wellbore inclination are derived from field data. Poisson's ratio, Biot's parameter, tensile strength, Young's modulus, and the friction angle are derived from the unsoaked experimental data in Table 1.

Table 2. Input data for modeling.

Model's Parameters	Values	Units
True vertical depth	3798	m
Overburden pressure	2.45	g/cm^3
Maximum horizontal stress	2.2	g/cm^3
Minimum horizontal stress	2.1	g/cm^3
Pore pressure	1.05	g/cm^3
The angle between the azimuth of the wellbore and the azimuth of the maximum horizontal stress	21.02	deg
Wellbore inclination	89	deg
Wellbore diameter	212.73	mm
Poisson's ratio	0.237	dimensionless
Biot's parameter	0.9	dimensionless
Tensile strength	0.8	MPa
Young's modulus	39	GPa
Friction angle	45.15	deg
Volumetric thermal expansion coefficient of rock matrix	2.59×10^{-5}	1/K
Wellbore wall temperature	423	K

5.1. Production Time and the Soaking Time of Formation Water

Through the study of the above immersion experiments, the results show that, in the case of the unimmersed rock core, if the critical production pressure difference is 2 MPa, according to Figure 9, open-hole completions without perforation pipes could be safe to produce until 2027. Meanwhile, in the case of two days of rock core immersion, the strength of the rock core is only able to be maintained up to the year 2026, and the strength of the rock core with seven days of core immersion decreases further, with strength only maintained up to 2025. In addition, the critical production pressure difference can reach up to 10.56 MPa without being soaked, while, for the rock strength of two days of core soaking, the critical production pressure difference decreases by 20.07%, and, at seven days of soaking, the ultimate production pressure difference decreases by 28.35%.

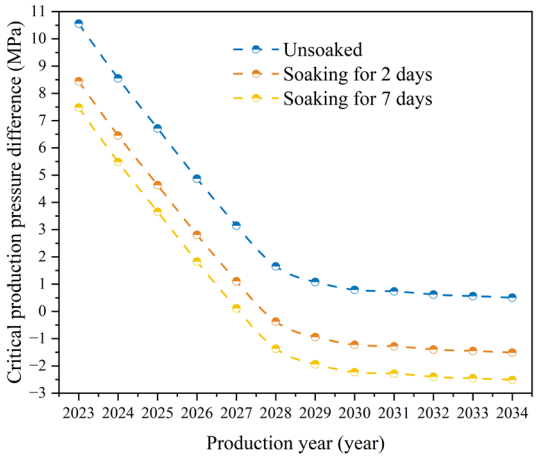

Figure 9. Change in critical production pressure difference with production year under different soaking times.

5.2. Well Inclination Angle

As shown in Figure 10, at the same well inclination angle, the critical production differential pressure tends to decrease year by year as the production year increases. Within the same production year, as the well inclination angle increases from 0° to 90°, the critical production pressure difference gradually decreases. This indicates that the wall stability of the horizontal section of the development well becomes progressively worse as the well inclination angle increases. Specifically, compared to the values in 2023, the critical production pressure difference range decreased from 21–25 MPa to 6–10 MPa by 2034, representing a reduction of 60% to 71%. This trend suggests that both a prolonged production time and an increased well inclination angle exacerbate wellbore instability, resulting in a significant narrowing of the allowable production pressure window. Therefore, effective measures are required to ensure wellbore stability under these conditions.

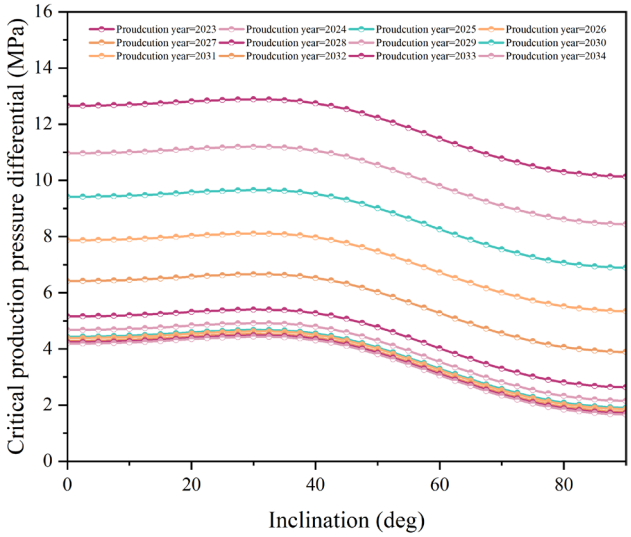

Figure 10. Change in the critical production pressure difference with production year under different inclination angles.

5.3. Cohesion

As shown in Figure 11, the cohesion of the rock reflects its strength, stability, and failure characteristics. Under the same azimuth conditions, the better the strength, stability, and destructiveness of the rock, the greater its cohesion, and the critical production pressure

difference also increases accordingly. When the cohesion of the rock is 25 MPa or 30 MPa, the critical production pressure difference remains positive across all azimuths, suggesting that normal production can be sustained using open-hole completion. However, when the cohesion decreases to 20 MPa, a production requirement of 5 MPa can only be met when the critical production pressure difference approaches 5 MPa along the direction of the minimum horizontal stress. If the cohesion is further reduced to 15 MPa, the critical production pressure difference becomes negative at all azimuths, indicating that open-hole completion can no longer maintain normal production.

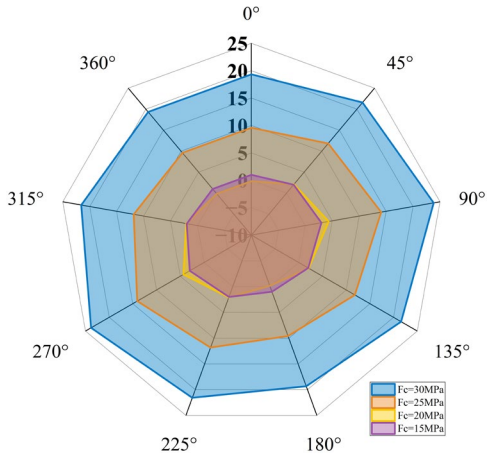

Figure 11. Variation in critical production pressure difference with cohesion in different directions.

5.4. Friction Angle

As shown in Figure 12, the internal friction angle of the rock is indicative of its shear resistance. Under consistent azimuth conditions, higher internal friction angles correspond to greater shear resistance, which in turn leads to an increase in the critical production pressure difference. When the internal friction angle is 30°, 35°, or 40°, the critical production pressure difference remains positive across all azimuths, indicating that open-hole completion can sustain normal production under these conditions. However, when the internal friction angle decreases to 15° or 20°, the critical production pressure difference becomes negative in all azimuths. This suggests that open-hole completion cannot maintain normal production under such conditions.

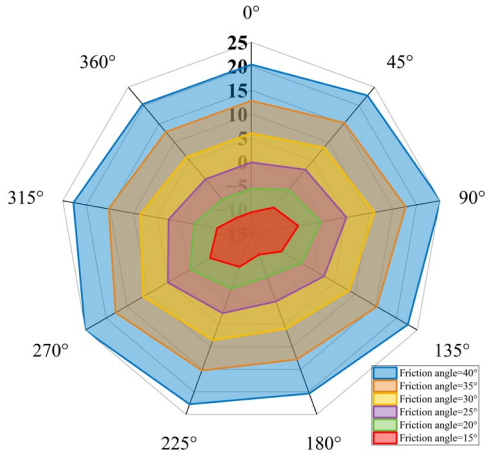

Figure 12. Variation in critical production pressure difference with internal friction angle in different directions.

5.5. Poisson's Ratio

As shown in Figure 13, the required bottomhole flowing pressure to maintain wellbore stability gradually decreases as Poisson's ratio decreases. This phenomenon suggests that a reduction in Poisson's ratio improves the rock's resistance to deformation, thereby reducing its susceptibility to shear failure and leading to an increase in the critical production pressure difference. However, the influence of Poisson's ratio on the critical production pressure difference is relatively modest. For Poisson's ratios of 0.1, 0.2, 0.3, and 0.4, the critical production pressure difference remains positive at all azimuths. This indicates that open-hole completion can be maintained under stable production conditions in these scenarios.

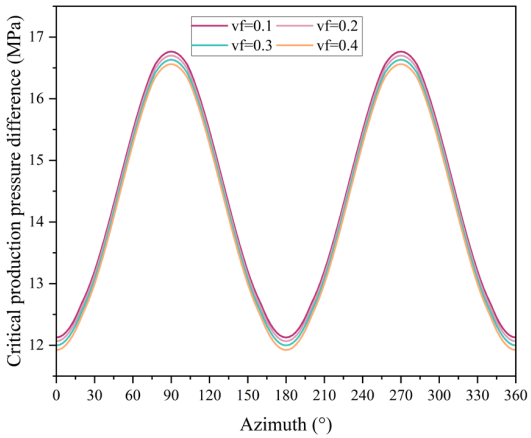

Figure 13. The variation of critical production pressure difference with Poisson's ratio in different directions.

5.6. In Situ Stress Nonuniformity

As shown in Figure 14, under a constant azimuth angle, the critical production pressure difference increases with the degree of in situ stress nonuniformity, represented by the ratio of the maximum to the minimum horizontal in situ stress. For all four stress ratios considered, the critical production pressure difference remains positive at every azimuth, suggesting that open-hole completion can be feasibly implemented under these conditions. However, at an azimuth of 90° and a stress anisotropy coefficient of 1.25, the critical production pressure difference is reduced by 4.5 MPa compared to the case where the coefficient is 1.1. This reduction indicates that increased nonuniformity of in situ stress may adversely affect wellbore stability, thereby lowering the critical production pressure difference.

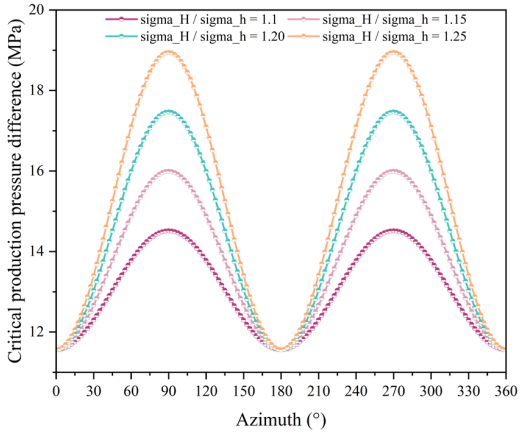

Figure 14. Variation in critical production pressure difference with nonuniformities of in situ stress in different directions.

5.7. Pore Pressure

As shown in Figure 15, under a constant azimuth angle, the critical production pressure difference increases with increasing pore pressure in the long horizontal open-hole section. When the pore pressure decreases to 23.5 MPa, the critical production pressure difference becomes negative for all azimuths except along the direction of the minimum horizontal in situ stress. This indicates that open-hole completion is not feasible under these conditions, and casing completion must be employed instead. These results highlight the significant influence of pore pressure on wellbore stability, particularly under low-pore-pressure conditions. In such scenarios, wellbore stability is considerably reduced, making open-hole completion incapable of meeting production requirements. Consequently, alternative reinforcement measures are necessary to ensure stable and efficient operations.

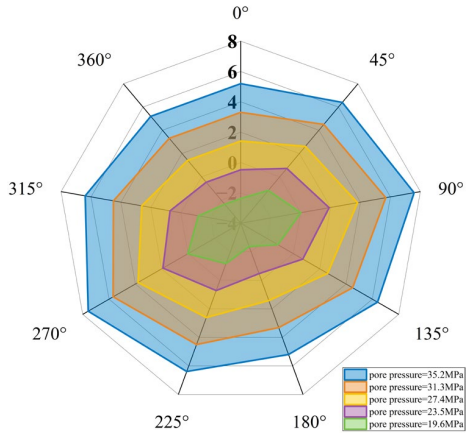

Figure 15. Variation in critical production pressure difference with pore pressure in different directions.

5.8. Biot Coefficient

As shown in Figure 16, under a fixed azimuth angle, the critical production pressure difference increases as the Biot coefficient decreases. For all five Biot coefficients presented, the critical production pressure difference remains positive across the entire range of azimuth angles. This suggests that the Biot coefficient is not a determining factor for the feasibility of open-hole completion in this stratum. These results demonstrate that, although the Biot coefficient influences wellbore stability to some extent, it does not play a decisive role in the practical application of open-hole completions. Other strata parameters, such as pore pressure and rock strength, are observed to have a more significant impact.

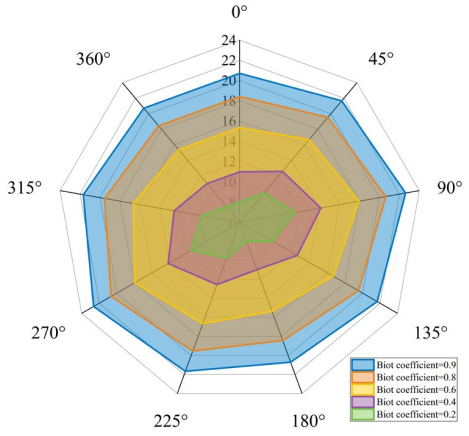

Figure 16. Variation in critical production pressure difference with the Biot coefficient in different directions.

6. Conclusions

(1) Based on rock mechanics experimental data and in situ stress evolution theory, a model for the critical production pressure difference in stable open-hole ultra-deep ERWs was established. The model was rigorously validated through field applications in three representative horizontal ERWs (*X*1, *X*2, and *X*3). The results show that, for the *X*1 well, the ultimate production pressure difference is much higher than the actual production pressure difference; thus, perforated pipes are not needed. In contrast, for wells *X*2 and *X*3, the ultimate production pressure difference, considering the confidence interval effects, is slightly higher or lower than the actual production pressure difference. Both wells have a risk of collapse and require perforated pipes, which aligns with the actual field completion situation.

(2) Immersion experiments showed significant differences in the critical production pressure difference between soaked and non-soaked conditions. Specifically, after soaking the rock core for two days, the ultimate production pressure difference decreased by 20.07% compared to the non-soaked baseline. After soaking for seven days, the ultimate production pressure difference decreased by 28.35% compared to the non-soaked rock core.

(3) A detailed analysis was conducted on the effects of key parameters, including the well inclination angle, cohesion, internal friction angle, Poisson's ratio, Biot coefficient, and pore pressure, on the critical production pressure difference in open-hole long horizontal sections. The results indicate that, as the well inclination angle increases, the critical production pressure difference decreases. Significant variations in the critical production pressure difference were observed with varying cohesion (30 MPa, 35 MPa, and 40 MPa) and internal friction angles (30° and 35°). As the internal friction angle increases, the ultimate production pressure difference also increases. In contrast, Poisson's ratio exhibits a comparatively small influence. Its effect is generally an order of magnitude less pronounced than that of cohesion or the internal friction angle under the studied conditions. Therefore, for practical design purposes in the target reservoir, Poisson's ratio can often be considered a secondary factor, whereas an increase in the Biot coefficient significantly reduces the critical production pressure difference. As the production years increase, the depletion of pore pressure leads to a significant narrowing of the pressure difference range.

This study provides theoretical support for well completion design in ultra-deep extended-reach wells, particularly for predicting wellbore stability and production pressure differences. The findings offer valuable guidance for similar wells in terms of completion design and risk assessment. However, future research could focus on the following areas: first, further optimization of model parameters, especially in relation to different geological conditions and well inclination angles; second, expanding experimental conditions to study the influence of various rock types and complex stress fields on critical pressure differences; and third, analyzing more complex real-world scenarios, such as the impact of multiphase flow, to enhance the model's applicability and accuracy.

Author Contributions: Methodology, J.Y.; Software, J.G., G.L., T.C. and J.Z.; Validation, J.G., G.L., Y.L., B.C., T.C. and J.Z.; Formal analysis, Y.L. and B.C.; Resources, X.C. and J.Y.; Writing—original draft, J.G., G.L., X.C., T.C. and J.Z.; Writing—review & editing, J.G., G.L., T.C. and J.Z.; Visualization, J.G. and G.L.; Supervision, Y.L., B.C., X.C. and J.Y.; Funding acquisition, X.C. and J.Y. All authors have read and agreed to the published version of the manuscript.

Funding: Key R&D Program of Shandong Province, China: 2022CXGC020406.

Data Availability Statement: The original contributions presented in this study are included in the article. Further inquiries can be directed to the corresponding authors.

Conflicts of Interest: Authors Junrui Ge, Yanfei Li and Bin Cai were employed by the company CNOOC (China) Limited Shanghai Branch. The remaining authors declare that the research was conducted in the absence of any commercial or financial relationships that could be construed as a potential conflict of interest.

Nomenclature

Symbol	Parameter Name (English)	Unit	First Appearing Equation
α_T	Volumetric thermal expansion coefficient of the rock matrix	1/K	Equation (2)
ΔP_p	Change value of pore pressure caused by exhaustion	MPa	Equation (5)
$\Delta\sigma_H$	Change value of maximum horizontal in-situ stress caused by pore pressure exhaustion	MPa	Equation (5)
$\Delta\sigma_h$	Change value of minimum horizontal in-situ stress caused by pore pressure exhaustion	MPa	Equation (5)
ΔT	Temperature change during the production process	°C	Equation (1)
θ	Circumferential angle around wellbore measured counter-clockwise from the x-axis	deg	Equation (12)
ν_t	Poisson's ratio	dimensionless	Equation (2)
σ_H	Maximum horizontal in-situ stress	MPa	Equation (7)
σ_h	Minimum horizontal in-situ stress	MPa	Equation (8)
σ_v	Overburden pressure (Vertical stress)	MPa	Equation (6)
σ_{rr}^T	Radial stress caused by temperature change in the wellbore	MPa	Equation (1)
$\sigma_{\theta\theta}^T$	Hoop stress caused by temperature change in the wellbore	MPa	Equation (1)
σ_{zz}^T	Axial stress caused by temperature change in the wellbore	MPa	Equation (1)
σ_{rr}	Radial stress around the wellbore including temperature and exhaustion of pore pressure's effects	MPa	Equation (12)
$\sigma_{\theta\theta}$	Hoop stress around the wellbore including temperature and exhaustion of pore pressure's effects	MPa	Equation (12)
σ_{zz}	Axial stress around the wellbore including temperature and exhaustion of pore pressure's effects	MPa	Equation (12)
$\tau_{r\theta}, r_{\theta z}, \tau_{rz}$	Components of shear stress around the wellbore include temperature and exhaustion of pore pressure's effects	MPa	Equation (12)
γ	Angle between the Z axis and the normal stress	deg	Equation (15)
$A - J$	Factors of coordinate conversion	dimensionless	Equation (14)
E_t	Young's modulus	GPa	Equation (2)
K	Temperature effect coefficient	MPa/°C	Equation (1)
L	Transformation matrix component	dimensionless	Equation (10)
P_p	Pore pressure	MPa	Equation (7)
r'	Radial distance	m	Equation (1)
X, Y, Z	Three factors of principal stresses	dimensionless	Equation (18)
α_p	Biot's parameter	dimensionless	Equation (7)
σ	Normal stress on a plane	MPa	Equation (15)
τ	Shear stress on a plane	MPa	Equation (15)
$\sigma_1, \sigma_2, \sigma_3$	Principal stresses	MPa	Equation (17)

References

1. Zhou, X.H.; Gao, S.L.; Gao, W.Z.; Li, N. Formation and distribution of marine-continental transitional lithologic reservoirsin Pingbei slope belt, Xihu sag, East China Sea Shelf Basin. *J. China Pet. Explor.* **2019**, *24*, 153–164. [CrossRef]
2. Liu, C.X.; Gao, H.Y.; Qin, D.W.; Xia, Y.; Shan, L.J. In-situ stress and rock mechanics analysis in the application ofhydraulic fracturing for horizontal wells in the low-permeability andtight sandstone gas reservoirs of the East China Sea. *J. World Pet. Ind.* **2024**, *31*, 78–89. [CrossRef]
3. Liu, Y.; Lin, C.Y.; Lin, J.L.; Huang, X.; Liu, B.B. Pore structure characteristics and genesis analysis of deep tight sandstone in Xihu Depression, East China Sea Basin. *J. Nat. Gas Geosci.* **2024**, *35*, 405–422.

4. Li, Q.; Qin, B.L.; Wang, J.H.; Xiong, Z.Y.; Ma, H.Y.; Wang, H.M. Practice analysis of open holesuspended sidetracking technology in XX low permeabilitygas field in EastChina Sea. *J. Pet. Geol. Eng.* **2021**, *35*, 75–81. [CrossRef]
5. Lei, L.; Li, Q.; Zhang, H.S.; Huang, Z. Practical Analysis of Horizontal Branch Well Technology in the East China Sea. *J. Offshore Oil* **2021**, *41*, 93–98. [CrossRef]
6. Xie, C.; Lv, Z.; Cheng, B.; Cai, Y.; Liao, Z.; Chen, Z. Porosity evolution and reservoir formation model of the Paleogene Huagang Formation sandstone in the YQ structure of the Xihu Depression, East China Sea Basin. *Mineral. Petrol.* **2025**, *45*, 122–139. [CrossRef]
7. Chen, X.Y.; Yang, J.; Gao, D.L.; Hong, Y.Q.; Zou, Y.Q.; Du, X. Unlocking the deepwater natural gas hydrate's commercial potential with extended reach wells from shallow water: Review and an innovative method. *Renew. Sustain. Energy Rev.* **2020**, *134*, 110388. [CrossRef]
8. Chen, X.Y.; Du, X.; Yang, J.; Gao, D.L.; Zou, Y.Q.; He, Q.Y. Developing offshore natural gas hydrate from existing oil & gas platform based on a novel multilateral wells system: Depressurization combined with thermal flooding by utilizing geothermal heat from existing oil & gas wellbore. *Energy* **2022**, *258*, 124870. [CrossRef]
9. Aadnoy, B.S. Modeling of the stability of highly inclined boreholes in anisotropic rock formations. *SPE Drill. Eng.* **1988**, *3*, 259–268. [CrossRef]
10. Ong, S.H.; Roegiers, J.C. Influence of anisotropies in borehole stability. *Int. J. Rock Mech. Min. Sci. Geomech. Abstr.* **1993**, *30*, 1069–1075. [CrossRef]
11. Lee, H.; Ong, S.H.; Azeemuddin, M.; Goodman, H. A wellbore stability model for formations with anisotropic rock strengths. *J. Petrol. Sci. Eng.* **2012**, *96*, 109–119. [CrossRef]
12. He, S.; Wang, W.; Zhou, J.; Huang, Z.; Tang, M. A model for analysis of wellbore stability considering the effects of weak bedding planes. *J. Nat. Gas Sci. Eng.* **2015**, *27*, 1050–1062. [CrossRef]
13. Li, Y.; Weijermars, R. Wellbore stability analysis in transverse isotropic shales with anisotropic failure criteria. *J. Petrol. Sci. Eng.* **2019**, *176*, 982–993. [CrossRef]
14. Li, M.b.; Liu, G.h.; Li, J. Thermal effect on wellbore stability during drilling operation with long horizontal section. *J. Nat. Gas Sci. Eng.* **2015**, *23*, 118–126. [CrossRef]
15. He, S.; Liang, L.X.; Zeng, Y.J.; Ding, Y.; Lin, Y.X.; Liu, X.J. The influence of water-based drilling fluid on mechanical property of shale and the wellbore stability. *Petroleum* **2016**, *2*, 61–66. [CrossRef]
16. Zhou, J.; He, S.M.; Tang, M.; Huang, Z.; Chen, Y.L.; Chi, J.; Zhu, Y.; Yuan, P. Analysis of wellbore stability considering the effects of bedding planes and anisotropic seepage during drilling horizontal wells in the laminated formation. *J. Petrol. Sci. Eng.* **2018**, *170*, 507–524. [CrossRef]
17. Wei, A.C.; Peng, X.S.; Han, C.; Li, Z.J.; Xu, F. Running technology for perforation pipe in the slim hole of the ffrst offshore HPHT horizontal well. *J. Oil Drill. Prod. Technol.* **2016**, *38*, 762–765. [CrossRef]
18. Fu, Y.; Pu, Y. Density of completion fluid for ultra deep wells in long naked eye horizontal sections analysis of the importance of wellbore stability. *J. Nat. Gas Technol. Econ.* **2024**, *18*, 15–19. [CrossRef]
19. Huang, X.S.; Li, Z.P.; Yan, K. Feasibility Evaluation of Open Hole Completion of Loose Sandstone Reservoir: Taking the Second Member of Shahejie Formation in the Second Area of Shengtuo Oilfield as an Example. *J. Sci. Technol. Eng.* **2023**, *23*, 2840–2847. [CrossRef]
20. Sun, J.X.; Ning, F.L.; Lei, H.W.; Gai, X.R.; Sánchez, M.; Lu, J.G.; Li, Y.L.; Liu, L.L.; Liu, C.L.; Wu, N.Y.; et al. Wellbore stability analysis during drilling through marine gas hydrate-bearing sediments in Shenhu area: A case study. *J. Petrol. Sci. Eng.* **2018**, *170*, 345–367. [CrossRef]
21. Wang, Y.L.; Dusseault, M.B. A coupled conductive–convective thermo-poroelastic solution and implications for wellbore stability. *J. Petrol. Sci. Eng.* **2003**, *38*, 187–198. [CrossRef]
22. Ma, T.S.; Chen, P.; Yang, C.H.; Zhao, J. Wellbore stability analysis and well path optimization based on the breakout width model and Mogi–Coulomb criterion. *J. Petrol. Sci. Eng.* **2015**, *135*, 678–701. [CrossRef]
23. Guo, Z.Y.; Wang, H.N.; Jiang, M.J. Elastoplastic analytical investigation of wellbore stability for drilling in methane hydrate-bearing sediments. *J. Nat. Gas Sci. Eng.* **2020**, *79*, 103344. [CrossRef]
24. Liu, H.B.; Cui, S.A.; Meng, Y.F.; Li, Z.; Yu, X.C.; Sun, H.R.; Zhou, Y.X.; Luo, Y. Rock mechanics and wellbore stability of deep shale during drilling and completion processes. *J. Petrol. Sci. Eng.* **2021**, *205*, 108882. [CrossRef]
25. Liu, C.; Zhou, F.B.; Kang, J.H.; Xia, T.Q. Application of a non-linear viscoelastic-plastic rheological model of soft coal on borehole stability. *J. Nat. Gas Sci. Eng.* **2016**, *36*, 1303–1311. [CrossRef]
26. Yousefian, H.; Soltanian, H.; Marji, M.F.; Abdollahipour, A.; Pourmazaheri, Y. Numerical simulation of a wellbore stability in an Iranian oilfield utilizing core data. *J. Petrol. Sci. Eng.* **2018**, *168*, 577–592. [CrossRef]
27. Rashidi, M.R.A.; Phuat, T.C.; Yakup, M.H. Openhole Completion Integrity Analysis for Life of CO_2 Injector Well. In Proceedings of the ARMA/DGS/SEG International Geomechanics Symposium, ARMA, Kuala Lumpur, Malaysia, 18–20 November 2024. ARMA-IGS-2024-0222. [CrossRef]

28. Chen, X.Y.; Gao, D.L.; Guo, B.; Feng, Y.C. Real-time optimization of drilling parameters based on mechanical specific energy for rotating drilling with positive displacement motor in the hard formation. *J. Nat. Gas Sci. Eng.* **2016**, *35*, 686–694. [CrossRef]
29. Merey, S. Well completion operations in gas hydrate reservoirs. *Int. J. Oil Gas Coal Technol.* **2019**, *20*, 373–396. [CrossRef]
30. Li, W.L.; Gao, D.L.; Yang, J. Study of mud weight window of horizontal wells drilled into offshore natural gas hydrate sediments. *J. Nat. Gas Sci. Eng.* **2020**, *83*, 103575. [CrossRef]
31. Chen, X.Y.; Yang, J.; Gao, D.L.; Feng, Y.C.; Li, Y.J.; Luo, M. The Maximum-Allowable Well Depth While Drilling of Extended-Reach Wells Targeting to Offshore Depleted Reservoirs. *Energies* **2018**, *11*, 1072. [CrossRef]
32. Chen, M.; Jin, Y.; Zhang, G.Q. *Petroleum Related Rock Mechanics*; Science Press: Beijing, China, 2008.
33. Chenevert, M.E.; Gatlin, C. Mechanical anisotropies of laminated sedimentary rocks. *SPE J.* **1965**, *5*, 67–77. [CrossRef]